Multi-Physical Simulations and Modelling of an Integrated GaN-on-Si Module Concept for Millimetre-Wave Communications

Kimmo Rasilainen[1], Koen Buisman[1], Kristoffer Andersson[2], and Christian Fager[1]
[1] Department of Microtechnology and Nanoscience, Chalmers University of Technology, SE-412 96 Gothenburg, Sweden
[2] Ericsson AB, SE-417 56 Gothenburg, Sweden
e-mail: kimmor@chalmers.se

***Abstract*—This paper presents a multi-physical system-level simulation workflow to characterise the performance of a heterogeneously integrated communications module for mm-wave applications. Basic principles behind modelling different parts and properties of the module are explained. The workflow combines the electromagnetic properties of a patch antenna array operating at 39 GHz with polynomial-based power amplifier (PA) models and thermal simulations of the structural heating. Effects of heating on the PA properties are also considered. The PA model is based on and compared with circuit simulations of a mm-wave transceiver chip, and the results are in good agreement. The proposed workflow can be used to describe and predict the performance of the module in different spatio-temporal use cases, and the approach also scales to larger arrays and more detailed simulation models.**

***Index Terms*—Antenna array, electrothermal model, heterogeneous integration, multi-physical, workflow.**

I. Introduction

The current rollout of fifth-generation (5G) communications systems marks a significant game changer for the wireless communications ecosystem. Compared to previous wireless systems, 5G promises to deliver, e.g., higher data rates and bandwidths, as well as a larger number of simultaneous users [1]. Due to spectral congestion, higher operating frequencies at mm-wave bands (roughly 30 GHz and beyond) are needed, as well as electrically beam-steerable multi-element antennas to switch between different users [2], [3]. Increasing path loss at higher frequencies calls for network densification, and deployment of a large number of small base stations helps to provide the required coverage.

Increased demand for better performance and higher functionality with as compact device size as possible is driving the development towards more and more integrated systems [4]–[6]. As a result, designers and engineers are faced with new challenges which partly arise from shrinking dimensions, the use of higher-order Multiple Input Multiple Output (MIMO) techniques, and from new requirements (higher frequencies and power levels, more complicated systems). Furthermore, the increase in integration and decrease in size can result in thermal problems, which means that careful consideration of suitable materials and thermal solutions is necessary [6], [7]. Therefore, it is important to understand the resulting multi-physical challenges and possible bottlenecks for the design and analysis of such integrated communications systems.

In general, the term *multi-physical* refers to a situation in which multiple coupled physical phenomena are analysed and modelled [8]: these can include, e.g., electro-thermal and thermo-mechanical models. Differences in the phenomena means that co-simulation is typically needed. In co-simulations, the various models are coupled and data exchange between simulation domains takes place (e.g., applying thermal simulation results as an input to electrical or circuit simulations). Recently, an overview of multi-physical aspects in electromagnetics has been presented in [9]. An example of a multi-physical problem relevant for the purpose of the current work is changes in the properties of the power amplifiers as a result of structural heating.

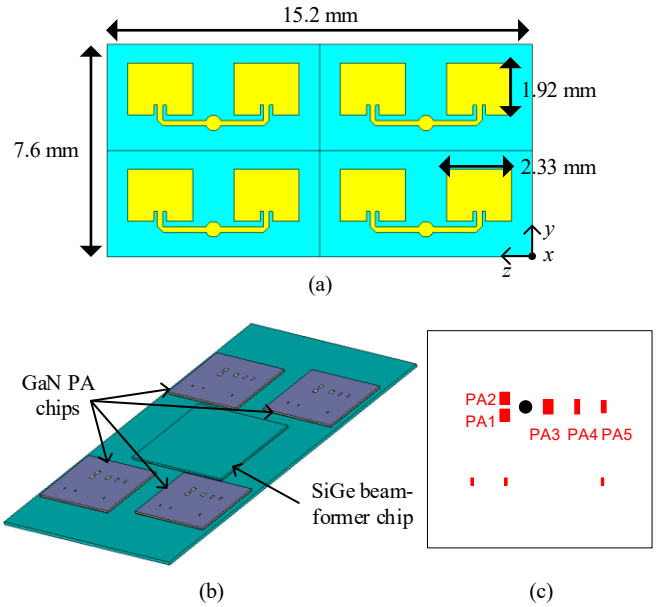

Fig. 1. Illustration of the analysed module design: (a) a 4×2 patch antenna array operating at 39 GHz (top view), (b) location of the PA and beamformer chips in the assembly, and (c) approximate transistor locations on the PA chip.

Technologicallly and commercially, the development of reliable and well performing multi-physical solvers and techniques is of great importance. In addition to being multi-physical, many of the relevant effects under study are also *multi-scale*, which means that the analysis needs to solve for effects that occur across multiple time and/or length scales [8]. In practice, this should be achieved in a reasonable computational time. As part of their effort to develop guidelines and visions for the future of electronic systems integration, the

Heterogeneous Integration Roadmap initiative has dedicated technical working groups on co-design for heterogeneous integration and on modelling and simulation [10].

II. Investigated Integrated Assembly

The investigated module utilises heterogeneous integration of gallium nitride on silicon (GaN-on-Si), which can enable a performance comparable to state-of-the art GaN-on-SiC processes while being more cost-effective [11]. Fig. 1 depicts the geometry of the used simulation model, and the material parameters assumed in the study are given in Table I.

The area of the module is $15.2\,\mathrm{mm} \times 7.6\,\mathrm{mm}$, and it contains four GaN-on-Si power amplifier (PA) chips and a silicon germanium (SiGe) beamformer chip, whose combined dissipated power (P_{diss}) may in the worst case exceed $30\,\mathrm{W}$. This means that the power density becomes very high, and a suitable and well-performing thermal management solution is therefore required. The largest power dissipation occurs at the PAs, and it is modelled using heat sources whose dimensions and placement correspond to those of individual transistors. This study does not take into account the power dissipated in the beamformer chip, although the effects of amplitude and phase tuning are considered later in this paper.

Each of the PA chips drives a two-element patch antenna whose targeted operating frequency is $39\,\mathrm{GHz}$, and altogether, the module has a 4×2 antenna array. The present study only considers the properties of a single four-antenna module, but the proposed workflow also generalises to larger arrays.

III. Multi-Physical Modelling Approach

A multi-physical modelling and simulation approach is used to investigate how the assembly geometry and materials, electrical and thermal effects in the power amplifiers, as well as the antenna characteristics affect the overall performance in a particular usage case. Fig. 2 presents a flow chart of the different steps involved in the study.

A. Characterising the Power Amplifiers

The characteristics of the power amplifiers (output signal and dissipated power) are described using polynomial-based models. These are an example of behavioural models that apply a mathematical dependency/model between certain input and output characteristics instead of considering the internal structure of the device under study [12].

With the modelling, the aim is to obtain a dynamic description of the PA behaviour during typical operating conditions in order to see how the PA output signal and dissipated power behave in the time domain as a function of input signal and temperature. In practice, both the amplitude and phase of a real PA differ from ideally linear amplitude and phase responses due to inherent nonlinearities. The amplitude- and phase-modulated (AM and PM) effects are described as AM/AM and AM/PM distortion [13].

The starting point for the modelling is simulated PA characteristics at different temperatures (here, 80, 27, and $-40\,^{\circ}\mathrm{C}$). The basic principle behind the polynomial PA models and their use together with antenna and thermal models is presented in [14]–[17]. Eqs. (1)–(2) represent the polynomials describing the dissipated power and output signal, respectively:

TABLE I
Thermal properties of the materials used in the study.

Material	Density $\rho\,(\mathrm{kg/m^3})$	Thermal conductivity $k\,(\mathrm{W/m{\cdot}K})$	Specific heat $C_p\,(\mathrm{J/kg{\cdot}K})$
Megtron 7	1820	0.4	0.88
Si	2330	148	0.7
SiGe	3950	8.8	0.5

$$P_{\mathrm{diss}}(|a_1|, T) = P_{\mathrm{dc}} + P_{\mathrm{in}} - P_{\mathrm{out}} = \sum_{p_{\mathrm{d}}=0}^{P_d} \xi_{p_d}(T)|a_1|^{p_d} \quad (1)$$

$$b_2(a_1, T) = \sum_{p_1=1}^{P_1} \alpha_{p_1}(T) a_1 |a_1|^{2(p_1-1)}. \quad (2)$$

In Eqs. (1)–(2), a_1 is the (time-dependent) PA input signal, and $\xi_{p_d}(T)$ and $\alpha_{p_1}(T)$ are real- and complex-valued temperature-dependent coefficients, respectively. The coefficient values depend linearly on the temperature, and they are initially determined at the three simulated temperatures. Beyond $80\,^{\circ}\mathrm{C}$, the coefficients are calculated using a spline extrapolation.

Fig. 3 shows the temperature dependence of the AM/AM, AM/PM, and dissipated power. The results show that the modelled and simulated results have a very good agreement. In the current study, the order of the dissipated power and output signal polynomials are $P_d = 8$ and $P_1 = 10$, respectively.

B. Thermal Equivalent Circuit Model

Transient and steady-state thermal properties of electronic systems can be represented using an analogy between electrical and thermal quantities. Electrical capacitance and resistance have their corresponding thermal counterparts, voltage (difference) is represented by temperature (difference), and electrical current is analogous to thermal power [18].

The composition of the thermal network is determined in part by the type of information that is of interest. Steady-state effects can be represented with a suitable network of thermal resistances, but capturing time-dependent transient effects also requires thermal capacitances. Different topologies can be applied to the networks, and depending on the choice of topology, the network may or may not take into account the internal physical structure of the modelled system.

Foster networks (parallel-coupled RC resonators in series) are mathematically simple to use both in time and frequency domain, and can be used to fit/represent the thermal response of a given structure using a certain number of stages. Eq. (3) gives the general time-domain expression for the impedance of a Foster network:

$$Z_{RC}(t) = \sum_{i=1}^{N} R_i(1 - \exp(-t/\tau_i)). \quad (3)$$

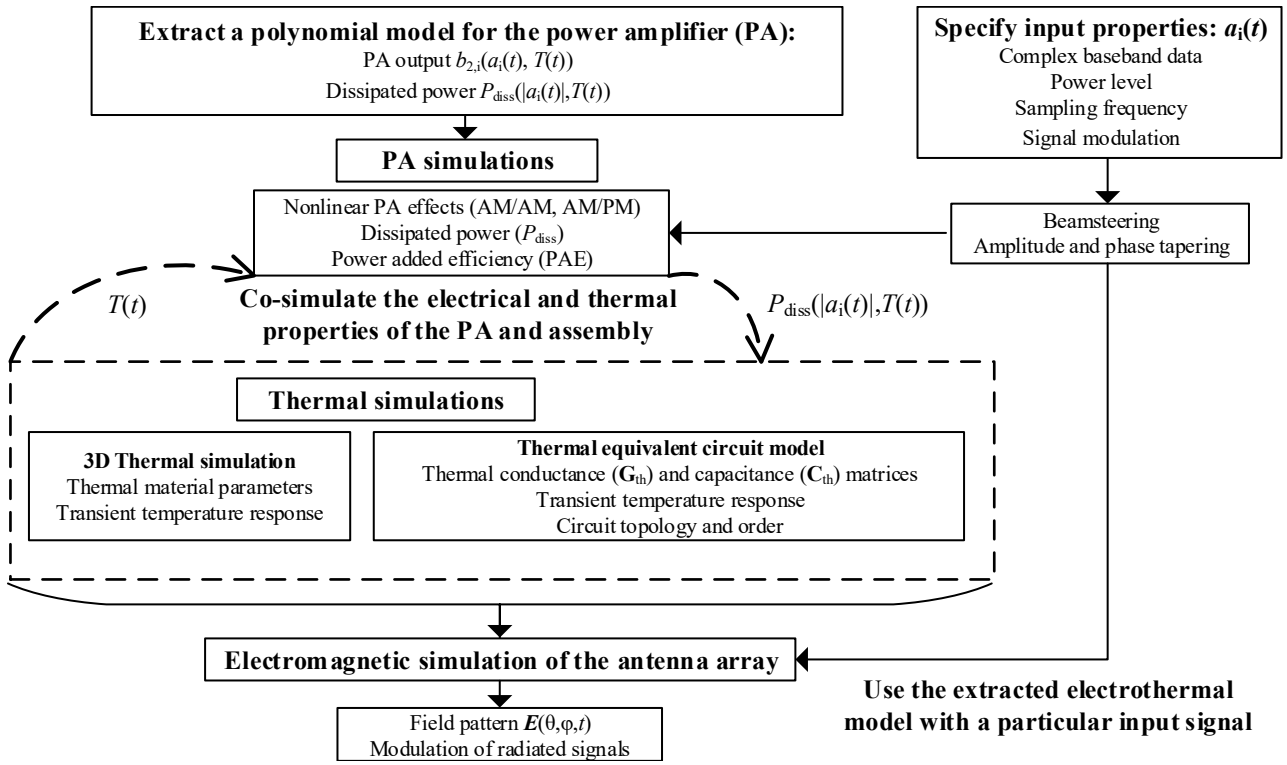

Fig. 2. Flow chart of the multi-physical simulation process used to characterise the system-level performance of the integrated GaN-on-Si module.

The required number of stages depends on the properties of the response and its different time scales (thermal time constant $\tau_{\mathrm{th}} = R_{\mathrm{th}}C_{\mathrm{th}}$). It should be noted that a thermal Foster network is not related to the internal structure. This is evident from the fact that the mutual order of two resonators can be changed and the resulting response remains the same for a particular input.

On the other hand, ladder-type Cauer networks have the thermal capacitances connected to a common thermal reference ground, and this type of network is more closely related to the physical nature of the structure. Unlike in the case of Foster networks, the precise mathematical representation of the Cauer network becomes very complicated, and the time constants depend on all thermal capacitances and resistances found in the network [19]. One approach to circumvent the problem of identifying the correct Cauer network is to initially determine the Foster network and to subsequently transform it to a Cauer network through formal identities [19].

The main focus of the present thermal analysis approach is to obtain a representative model for the thermal effects observed in the simulations rather than a highly detailed description of the internal structure of the assembly. Therefore, a Foster network is used to describe the thermal transient response, and a third-order network (three thermal time constants) appears sufficient to accurately reproduce the transient response.

The network is depicted in Fig. 4, and the corresponding element values and thermal time constants are given in Table II. As the network is in this case linear, it is able to capture the thermal response also with varying power levels or when pulsed input signals are used. In a more general case, the thermal response is affected by properties such as temperature-dependent semiconductor material parameters. This effect is neglected in the present work to simplify the modelling.

In order to calculate the transient thermal response using the equivalent circuit model, numerical integration of the temperature given by the circuit as a function of dissipated power is required. The following forward Euler type expression is used for the circuit of Fig. 4:

$$\mathbf{T}_{n+1} = \mathbf{C}_{\mathrm{th}}^{-1}\Big((\mathbf{T}_n - T_{\mathrm{amb}})\,(\mathbf{C}_{\mathrm{th}} - \Delta t\mathbf{G}_{\mathrm{th}}) + \Delta t\mathbf{P}_{\mathrm{diss},n}\Big) + T_{\mathrm{amb}}, \quad (4)$$

in which Δt is the length of the timestep used and T_{amb} is the ambient temperature. This expression is obtained by solving the circuit equations of the RC network with nodal analysis and utilising the aforementioned electrothermal analogy. More details on the mathematics involved is found in [16].

The thermal conductance $(\mathbf{G}_{\mathrm{th}})$ and capacitance $(\mathbf{C}_{\mathrm{th}})$ matrices are

$$\mathbf{G}_{\mathrm{th}} = \begin{pmatrix} G_1 & -G_1 & 0 \\ -G_1 & G_1+G_2 & -G_2 \\ 0 & -G_2 & G_2+G_3 \end{pmatrix} \quad (5)$$

and

$$\mathbf{C}_{\mathrm{th}} = \begin{pmatrix} C_1 & -C_1 & 0 \\ -C_1 & C_1+C_2 & -C_2 \\ 0 & -C_2 & C_2+C_3 \end{pmatrix}, \quad (6)$$

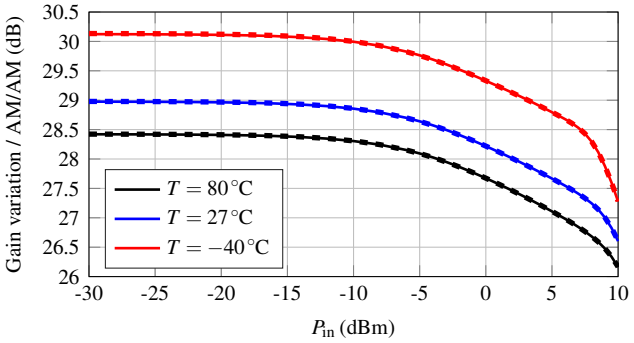

(a)

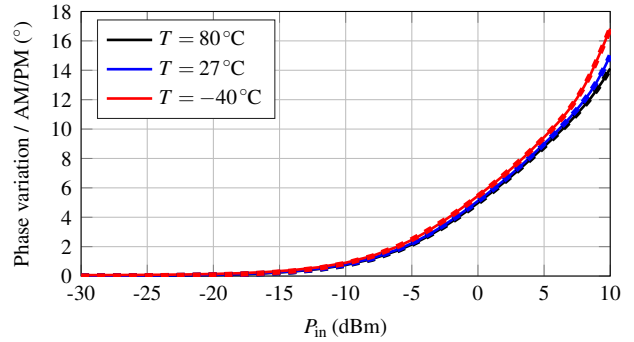

(b)

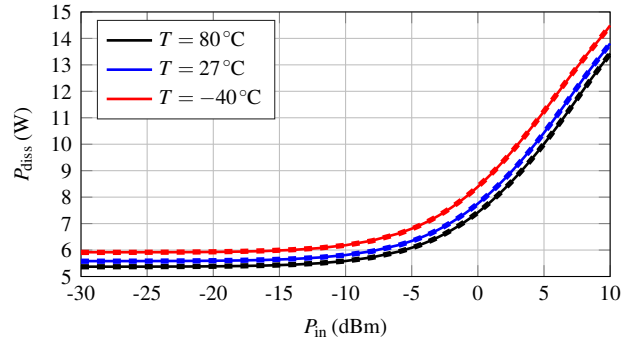

(c)

Fig. 3. Modelled and simulated power amplifier (PA) characteristics at three different temperatures: (a) gain variation / AM/AM, (b) phase variation / AM/PM, and (c) dissipated power (P_{diss}). Solid and dashed lines represent modelled and simulated results, respectively.

in which $G_i = R_i^{-1}$. The circuit elements, the values of which are given in Table II, follow the labeling used in Fig. 4.

C. Simulated Antenna Characteristics

Analysis of the combined performance of the investigated module requires taking into account the properties of the antenna array. Fig. 1(a) shows the 4×2 array of patch antennas in which the two-element patches form a subarray. The operating frequency of the antennas is 39 GHz, and the impedance matching and worst-case mutual coupling between the four antenna elements is presented in Fig. 5.

At the desired frequency, the return loss is approximately 10 dB, and the worst-case mutual coupling also remains at

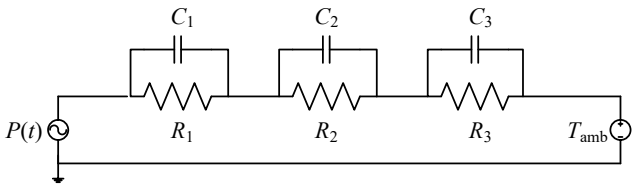

Fig. 4. Thermal Foster-type RC equivalent circuit used to model the heating of the GaN-on-Si PA chip.

TABLE II
ELEMENT VALUES AND TIME CONSTANTS FOR THE CIRCUIT OF FIG. 4.

$R_1 = 12\,\text{K/W}$	$C_1 = 14\,\text{mJ/K}$	$\tau_1 = 168\,\text{ms}$
$R_2 = 8.2\,\text{K/W}$	$C_2 = 3\,\text{mJ/K}$	$\tau_2 = 24.6\,\text{ms}$
$R_3 = 7.6\,\text{K/W}$	$C_3 = 0.5\,\text{mJ/K}$	$\tau_3 = 3.8\,\text{ms}$

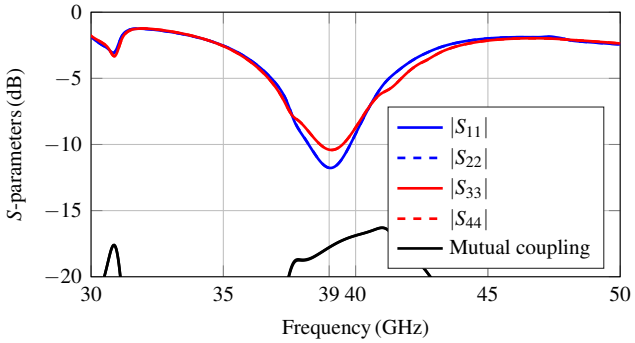

Fig. 5. Simulated S-parameters of the investigated 4×2 antenna array operating at 39 GHz.

a reasonable level. The radiation pattern ($\boldsymbol{E}$ field) of the antenna array with respect to the module and without any beam steering is shown in Fig. 6. In this case, all antenna elements are fed in-phase and with a unity excitation.

D. Input Signal Characteristics

As the input signal, a Long Term Evolution (LTE) communications signal with a 20-MHz bandwidth and 64QAM modulation is used in the simulations. The signal is complex-valued, and its magnitude is normalised to a specified input power level, which in the following simulations is 4 dBm.

This signal serves as an example of a realistic communications signal even though it is more narrowband than the 5G signals that could be used during the actual operation of such a module. The communications scenario considered is transmission (downlink only) from the 4×2 array (acting as the base station) to the user equipment.

IV. Simulated Multi-Physical Characteristics

In order to understand how the radiated fields at different time instants and directions are affected by the electrothermal properties of the PAs and the module, the previous electrical and thermal simulation models are combined with electromag-

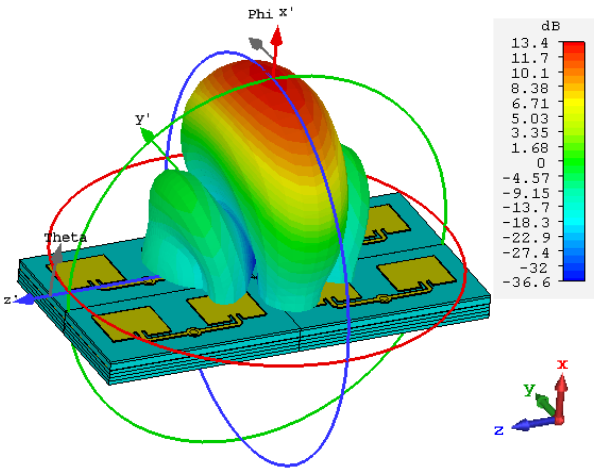

Fig. 6. Simulated $\boldsymbol{E}$ field pattern of the 4×2 antenna array at 39 GHz. All antennas are fed in-phase and with a unity excitation.

netic simulations of the 4×2 antenna array. This procedure follows the workflow presented in Fig. 2.

A. Transient Thermal Response

In the assembly, the GaN-on-Si PA chips and the SiGe beamformer chip are encased in a dielectric/substrate, the material of which is Megtron 7. The current simulation model only includes the substrate layers and the chips, and details of the various metal parts (such as transmission lines, signal vias, and ground planes) are not considered. Under these assumptions, the heat spreading capabilities of the module and consequently the properties of the PA can be affected, especially due to the low themal conductivity of Megtron 7 (see Table I). The inclusion of thermal vias and other metal structures to enhance the vertical and lateral heat spreading will improve the situation and reduce the temperature at the PAs and other parts of the assembly.

Fig. 7 depicts the transient thermal response of the five transistors PA1–PA5 at their center points. These results are obtained from 3D thermal simulations in CST Microwave Studio. In this case, the total dissipated power is $P_{\mathrm{diss,tot}} = 7\,\mathrm{W}$. For comparison, the response given by an ADS transient simulation of the equivalent circuit of Fig. 4 is also shown. The agreement between the two simulation methods is good.

To represent the PA chip with a simplified model, a representative "figure of merit" is required to describe the overall thermal response. In principle, it is possible to choose this representation in a variety of different ways, and here the temperature at the geometric center point of the three largest transistors is used (indicated by the black dot in Fig. 1(c)). The temperature at this point is given by the dotted black line in Fig. 7. When looking at the curves of Fig. 7, it can be seen that transistors PA1–PA3 heat up the most. This is expected since these three transistors are also the largest ones.

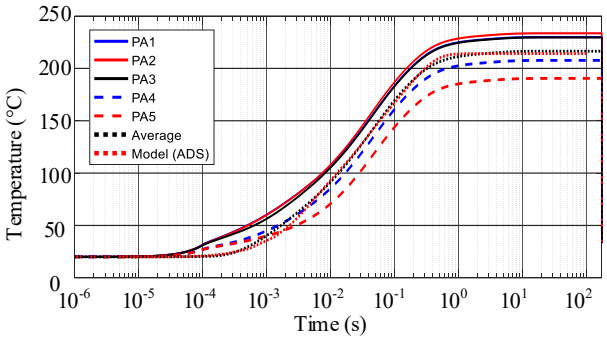

Fig. 7. Transient thermal response of the individual transistors (PA1–PA5), the response at the geometric average location, and the response given by ADS using the equivalent circuit of Fig. 4.

B. Structural Heating

During practical operating conditions, the radiated signals and dissipated power are not constant but are rather affected by the time-dependent input signal and communications scheme (pulsing of the signal etc.). As a result, the structure and PA exhibit a heating and cooling cycle, and the temperature drop depends on the duration of the low-power state (in which the power is either switched off or reduced from its peak value).

Fig. 8 illustrates how the peak temperature of the PA behaves when it is switched on and off during successive cycles. In this case, the input signal during the off state is zero, and during the on cycle, the input signal relates to an input power of 4 dBm. With the present pulsing and duration of the calculation, the temperature more or less reaches steady state at the end of the cycle (both in the on and off states of the PA). When the amplifier is switched off, it cools down approximately 20 °C before heating up again. During the on-stage, the small ripple in the temperature profile is a result of the time-dependent variations in signal amplitude.

The amount the temperature drops is limited by the fact that the dissipated power remains rather high (in the order of watts, as seen in Fig. 3(c)) and does not immediately tend to zero once the input signal is zero. In actual operating conditions, in the off mode, the dc supplies are likely also switched off, which helps to lower the average temperature. The temperature cycle presented in Fig. 8 is intended to act as a proof-of-concept result to show that the current simulation workflow is able to follow the characteristics of time-dependent input signals. In more detailed models, factors such as the switching time between transmission and reception in Time Division Duplexing (TDD) systems should be accounted for. Typically, these changes take place in the microsecond range.

C. Beamsteering of the Array and Time-Dependent Combined Electric Field

When combining the input signals, the PA model, and the antennas, the same input signal is fed to all four PA branches. In the present model, there is no thermal coupling between different branches and, as a result, the model combining essentially reduces to feeding the same PA output signal to

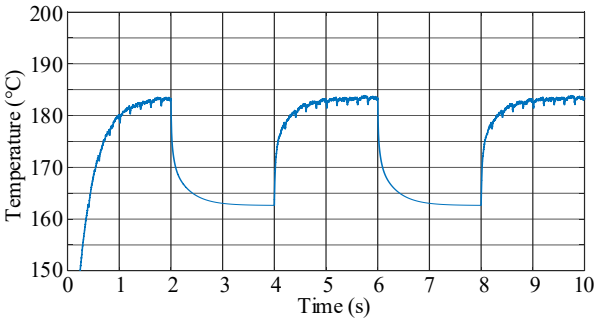

Fig. 8. Transient temperature profile of the PA during five cycles of pulsed operation. In this case, $P_{\text{in}} = 4\,\text{dBm}$ and the PA is switched off during the even cycles (2 and 4).

all four antenna ports, with a possibility of beamsteering through amplitude and phase tapering. Amplitude tapering mainly affects the pattern shape (beamwidth, side lobe level) and the direction of the main and/or side lobes can be changed by altering the phase.

Fig. 9 shows an example of the $\boldsymbol{E}$ field pattern without and with beamsteering. In the latter case, the main lobe is steered to the direction $\theta = 105°$, $\phi = 335°$. Here, the antennas are fed a signal amplified by the PA, as shown by the differences in the scales of Figs. 6 and 9. It can be seen that in addition to the main beam direction, also the direction and strength of the side lobes are affected. In a particular usage scenario, the combined effects of amplitude and phase tuning (in practice with the beamformer chip) need to be considered to point the radiation pattern towards the intended user(s) with as little interference/radiation towards unwanted directions as possible.

Fig. 10 illustrates the time-dependent behaviour of the magnitude of $\boldsymbol{E}_\theta$ and $\boldsymbol{E}_\phi$ field components in the main lobe direction of Fig. 9(b). The curves shows that, in addition to the variation of the $\boldsymbol{E}_\phi$ component with the input signal, this field component is significantly stronger than the $\boldsymbol{E}_\theta$ component. This happens because the polarisation of the antenna array is linear, and in the present configuration $\boldsymbol{E}_\phi$ and $\boldsymbol{E}_\theta$ are the co- and cross-polarised components, respectively.

When extending the current simulation model to a more detailed one, it could be interesting to study how the array pattern varies as a function of time due to dissimilarities in individual PA branches. Examples of these include amplitude variations in different PAs, differences in temperature profile due to the position within the array, and thermal and electrical coupling from other branches. Currently, the time-dependent effects in the $\boldsymbol{E}$ field are caused by the input signal and PA properties, and the effect of the array configuration is not included in the model.

V. Conclusion

This study has presented a multi-physical approach to simulate and model different parts of an integrated mm-wave communications system module. General properties and challenges of multi-physical analysis as well as behavioural and

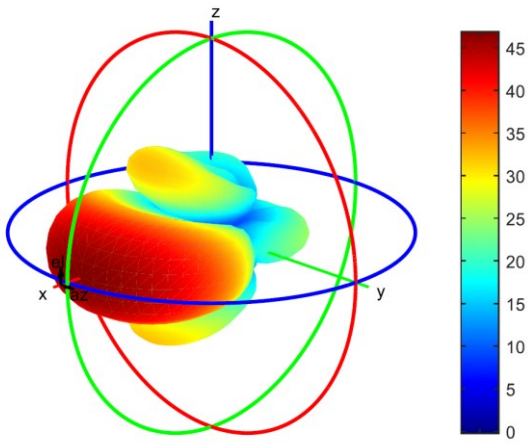

(a)

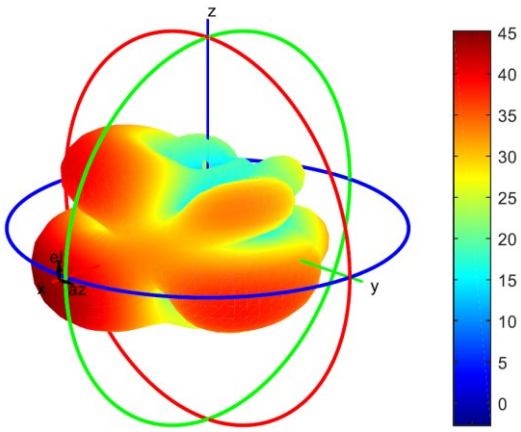

(b)

Fig. 9. Simulated 3D $\boldsymbol{E}$-field patterns of the 4×2 antenna array (a) without beam steering (main beam direction $\theta = 90°$, $\phi = 0°$) and (b) with the main beam steered towards the direction $\theta = 105°$, $\phi = 335°$. The antennas are fed with a signal amplified by the PA with amplitude and phase tapering.

thermal modelling have also been described. A comparison of the modelled and simulated results shows that they are generally in good agreement. The basic workflow currently considers the properties of a single four-element array with simplifications (no memory effects in the PAs, no thermal coupling between individual paths etc.), but the same approach can also be applied to more detailed package and PA models.

Regarding the accuracy and validity of the different parts in the current analysis approach, the biggest source of uncertainty likely relates to the thermal modelling. In part, this is due to a fairly simple 3D thermal simulation model (substrate layers and circuit chips), and in part due to the way in which the self and mutual heating of the individual transistors is reduced to a temperature profile at a particular location. Although useful from a practical point of view, the ambiguity in the choice of

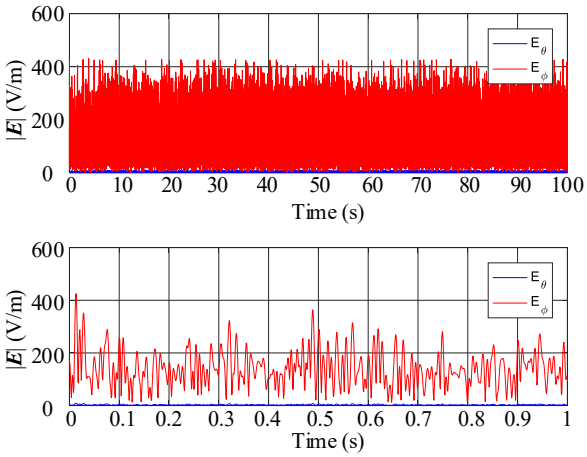

Fig. 10. Temporal variation of the electric field magnitude ($|\boldsymbol{E}|$) in direction $\theta = 105°$, $\phi = 335°$ when the main beam is steered to that direction.

location presents a possibility to under- or overestimate the thermal characteristics of the power amplifiers.

In the future, the current simulation models can be extended to include more details and characteristics of the different subassemblies of the module to increase the accuracy of the analysis. Additionally, it is possible to update the current simulation model to higher frequencies (such as E/W-band) by modifying the amplifier and antenna models.

ACKNOWLEDGEMENT

This work was carried out in the SERENA project, which has received funding from the European Union's Horizon 2020 research and innovation programme under grant agreement No. 779305. The authors would like to thank OMMIC for providing the simulation data for the power amplifiers and Fraunhofer IZM for providing the 3D model of the assembly.

REFERENCES

[1] J. G. Andrews *et al.*, "What will 5G be?" *IEEE J. Sel. Areas Commun.*, vol. 32, no. 6, pp. 1065–1082, Jun. 2014.

[2] K. Kibaroglu, M. Sayginer, and G. M. Rebeiz, "A low-cost scalable 32-element 28-GHz phased array transceiver for 5G communication links based on a 2×2 beamformer flip-chip unit cell," *IEEE J. Solid-State Circuits*, vol. 53, no. 5, pp. 1260–1274, May 2018.

[3] X. Gu *et al.*, "Development, implementation, and characterization of a 64-element dual-polarized phased-array antenna module for 28-GHz high-speed data communications," *IEEE Trans. Microwave Theory Tech.*, vol. 67, no. 7, pp. 2975–2984, Jul. 2019.

[4] I. Ndip and K.-D. Lang, "Roles and requirements of electronic packaging in 5G," in *Proc. 7th Electronic System-Integration Technology Conf. (ESTC)*, Dresden, Germany, Sep. 2018, pp. 1–5.

[5] R. Guggenheim and L. Rodes, "Roadmap review for cooling high-power GaN HEMT devices," in *Proc. 2017 IEEE Int. Conf. Microwaves, Antennas, Communications and Electronic Systems (COMCAS)*, Tel Aviv, Israel, Nov. 2017, pp. 1–6.

[6] S. V. Garimella *et al.*, "Thermal challenges in next-generation electronic systems," *IEEE Trans. Compon. Packag. Technol.*, vol. 31, no. 4, pp. 801–815, Dec. 2008.

[7] K. Rasilainen, P. Ingelhag, P. Melin, T. M. J. Nilsson, M. Thorsell, and C. Fager, "Thermal characteristics of vertically-integrated GaN/SiC-on-Si assemblies: A comparative study," in *Proc. IEEE 69th Electronic Components and Technology Conf. (ECTC)*, Las Vegas, NV, USA, May 2019, pp. 1405–1412.

[8] C. Bailey and S. Stoyanov, "Co-simulation and modelling for heterogeneous integration of high-tech electronic systems," in *Proc. 40th Int. Spring Seminar Electronics Technology (ISSE)*, Sofia, Bulgaria, May 2017. ISSN 2161-2536 pp. 1–5.

[9] J.-M. Jin and S. Yan, "Multiphysics modeling in electromagnetics: Technical challenges and potential solutions," *IEEE Antennas Propagat. Mag.*, vol. 61, no. 2, pp. 14–26, Apr. 2019.

[10] "Heterogeneous Integration Roadmap (2019 Edition)," 2019. [Online]. Available: https://eps.ieee.org/technology/heterogeneous-integration-roadmap/2019-edition.html

[11] L. Cao, C.-F. Lo, H. Marchand, W. Johnson, and P. Fay, "Coplanar waveguide performance comparison of GaN-on-Si and GaN-on-SiC substrates," in *Proc. IEEE Compound Semiconductor Integrated Circuit Symp. (CSICS)*, Miami, FL, USA, Oct. 2017. ISSN 2374-8443 pp. 1–4.

[12] J. C. Pedro and S. A. Maas, "A comparative overview of microwave and wireless power-amplifier behavioral modeling approaches," *IEEE Trans. Microwave Theory Tech.*, vol. 53, no. 4, pp. 1150–1163, Apr. 2005.

[13] D. Schreurs, M. O'Droma, A. A. Goacher, and M. Gadringer, *RF Power Amplifier Behavioral Modeling*. Cambridge University Press New York, NY, USA, 2008.

[14] C. Fager, X. Bland, K. Hausmair, J. C. Cahuana, and T. Eriksson, "Prediction of smart antenna transmitter characteristics using a new behavioral modeling approach," in *Proc. IEEE MTT-S Int. Microwave Symp. (IMS2014)*, Jun. 2014. ISSN 0149-645X pp. 1–4.

[15] C. Fager, K. Hausmair, T. Eriksson, and K. Buisman, "Analysis of thermal effects in active antenna array transmitters using a combined em/circuit/thermal simulation technique," in *Proc. Integrated Nonlinear Microwave and Millimetre-wave Circuits Workshop (INMMiC)*, Taormina, Italy, Oct. 2015, pp. 1–3.

[16] E. Baptista, "Analysis of electrical and thermal coupling effects in integrated MIMO transmitters," Master's Thesis, Instituto Superior Técnico, Lisbon, Portugal and Chalmers University of Technology, Gothenburg, Sweden, May 2017.

[17] E. Baptista, K. Buisman, J. C. Vaz, and C. Fager, "Analysis of thermal coupling effects in integrated MIMO transmitters," in *Proc. IEEE MTT-S Int. Microwave Symp. (IMS)*, Honolulu, HW, USA, Jun. 2017, pp. 75–78.

[18] M. Iachello *et al.*, "Lumped parameter modeling for thermal characterization of high-power modules," *IEEE Trans. Compon. Packag. Manuf. Technol.*, vol. 4, no. 10, pp. 1613–1623, Oct. 2014.

[19] S. Russo, "Measurement and simulation of electrothermal effects in solid-state devices for RF applications," Ph.D. dissertation, University of Naples Federico II, Naples, Italy, 2011.